ELSEVIER

Chemical Engineering Science 61 (2006) 3313–3322

Chemical Engineering Science

www.elsevier.com/locate/ces

CFD modeling of gas dispersion and bubble size in a double turbine stirred tank

F. Kerdouss, A. Bannari, P. Proulx*

Department of Chemical Engineering, Université de Sherbrooke, Sherbrooke, Que., Canada J1K 2R1

Received 22 February 2005; received in revised form 19 October 2005; accepted 29 November 2005
Available online 31 January 2006

Abstract

In the present paper, gas dispersion in a double turbine baffled stirred tank is modeled using a commercial computational fluid dynamics (CFD) code FLUENT 6.1 (Fluent Inc., USA). A bubble number density equation is implemented in order to account for the combined effect of bubble break-up and coalescence in the tank. In the proposed work, the impellers are explicitly described in three dimensions using multiple reference frame model. Dispersed gas and bubbles dynamics in the turbulent water are modeled using an Eulerian–Eulerian approach with dispersed k–ε turbulent model and modified standard drag coefficient for the momentum exchange. The model predicts spatial distribution of gas holdup, average local bubble size and flow structure. The results are compared with experimental and numerical finding reported in the literature and good agreement between the present model and measurements of Alves et al. [Gas liquid mass transfer coefficient in stirred tanks interpreted through bubble contamination kinetics. Chemical Engineering Science, 2002, 57, 487–496] is achieved.

Keywords: Computational fluid dynamics (CFD); Multiphase flow; Bubble size; Gas dispersion; Mixing; Stirred tank

1. Introduction

Stirred tank reactors are widely used in chemical and biochemical processes to carry out a variety of operations, like homogenization, gas dispersion, heat transfer and solid suspension. Over the years many experimental studies have been made to investigate the characteristics of gas dispersion in stirred tank as it influences the mass transfer effectiveness. These studies usually result in a correlation that relates the global performances to operating conditions and geometry. However, these correlations do not reflect the details of the physics involved in mass transfer and are only applicable in the narrow range of operating conditions for which they were determined. Several recent publications have established the potential of computational fluid dynamics (CFD) for describing the hydrodynamics of stirred tank and improving the knowledge of local information about turbulent flow field, gas-holdup, interfacial area, bubble size and reaction rates (Bakker and Van Den Akker, 1994; Hjertager, 1998; Lane et al., 2005, 2002). Various approaches have been used, generally using an Euler–Euler approach with only constant bubble size in order to predict gas holdup and flow field (Deen et al., 2002; Friberg, 1998; Morud and Hjertager, 1996; Ranade and Deshpande, 1999; Ranade, 1997). Prediction of local bubble size and local gas holdup was carried by Bakker and Van Den Akker (1994) and Venneker et al. (2002) using, respectively, a conservation equation of bubble volume and population balance equations for turbulent gas dispersion in stirred tanks. However, the two-phase flow field and turbulence properties were simulated in one-way coupling by scaling single-phase flow obtained by CFD simulations and the impeller was modeled with imposed boundary conditions via experimental data. Often, this data is too difficult to obtain in the case of multiphase flow and does not capture the details of the flow between the impeller blades which is essential for a realistic simulation (Ranade, 1997). Lane et al. (2002) have carried out a thorough three-dimensional CFD simulation to model a gas sparged tank equipped with a single Rushton turbine using multiple reference frame (MRF) model for the impeller and bubble number density equation, including various expressions for drag and dispersion forces. Their results indicate the correct patterns of liquid velocity, gas distribution and

* Corresponding author. Tel.:+1 819 821 8000x2173; fax: +1 819 821 7955.
E-mail address: pierre.proulx@usherbrooke.ca (P. Proulx).

0009-2509/$ - see front matter © 2005 Elsevier Ltd. All rights reserved.
doi:10.1016/j.ces.2005.11.061

bubble size through the tank; however, the bubble sizes were underpredicted and gas holdup was overpredicted. Recently, Alves et al. (see Alves et al., 2004, 2002a,b; Vasconcelos et al., 1995) have given detailed informations about gas dispersion in a double turbine stirred tank. In their work, local gas holdups, local bubble size distributions, local interfacial area were measured at different mixing speeds in both coalescing and noncoalescing medias. Their modeling was achieved with a simple compartment model, based on experimental work, divided into 30 compartments where the flow rates between their interfaces was given as function of the pumping flow rate. The model predicts in reasonable agreement bubble size and local gas holdup. Turbulent data required in bubble number density equation however were taken from literature and the model fails in predicting the breakage and it requires bubble size input at the impeller tip. The aim of this work is to use a full three-dimensional CFD approach to model the experiments of Alves et al. (2002a). Both multiphase turbulent flow, impeller rotation, gas bubble break-up and coalescence phenomena are modeled. The CFD predictions are compared quantitatively with experiments.

2. Numerical model

2.1. Tank specifications and numerical technique

The solution domain for the experimental system of Alves et al. (2002a), investigated in this work, is shown in Fig. 1. It consists of a flat bottom stirred cylindrical vessel with diameter T of 0.292 m and liquid height $H = 2T$. A double six bladed standard Rushton impellers with diameter of $D = T/3$ were located respectively at 0.146 and 0.438 m above the tank base. The impeller blade width, l, and the impeller blade height, w, are equal respectively to $D/4$ and $D/5$. The tank is equipped with four baffles of $0.1T$ width uniformly spaced around the periphery. Gas is supplied through a small sparger, which is located between the tank base and the lower impeller. In the present paper, numerical simulations are compared to the experimental data (Alves et al., 2002a) of a stirred tank filled with tap water with a total height of 0.584 m, gas flow rate of $1.67 \times 10^{-4}\,\mathrm{m^3\,s^{-1}}$ and an impeller rotation speed of $7.5\,\mathrm{s^{-1}}$ corresponding to a turbulent *Reynolds number*, $Re = \rho_L N D^2/\mu_L = 7.1 \times 10^4$. The water properties are set as $\rho_L = 998.2\,\mathrm{kg\,m^{-3}}$, $\mu_L = 0.001\,\mathrm{kg\,m^{-1}\,s^{-1}}$ and $\sigma = 0.073\,\mathrm{N\,m^{-1}}$. The properties of air are set as $\rho_G = 1.225\,\mathrm{kg\,m^{-3}}$, $\mu_G = 1.789 \times 10^{-5}\,\mathrm{kg\,m^{-1}\,s^{-1}}$. To reduce the computational requirements and numerical efforts, the flow domain is divided into two symmetric parts and only one part is modeled including two thin baffles and three thin impeller blades for each turbine (see also Deen et al., 2002; Khopkar et al., 2005; Ranade and Deshpande, 1999). Using one quarter model containing just one blade and one baffle will represent a tank with six baffles rather than four. The effect of the extra baffling may be minimal (Lane et al., 2005) but as we want to take the plane of measurement in mid-baffles, the configuration of 180 degrees is chosen here. The geometry of the shaft is not included in the present model and therefore its influence on the flow field is ignored. The FLUENT preprocessor GAMBIT 2 (2004) is used as geometry and mesh generator. Fig. 2 shows the essential features of the 280 000 tetrahedral cells, generated for the tank. The quality of meshes was analyzed using the skewness criteria based on the difference between the cell size and the optimal size which is the equilateral volume. All the cells skewness are below 0.70 which indicate that the mesh is

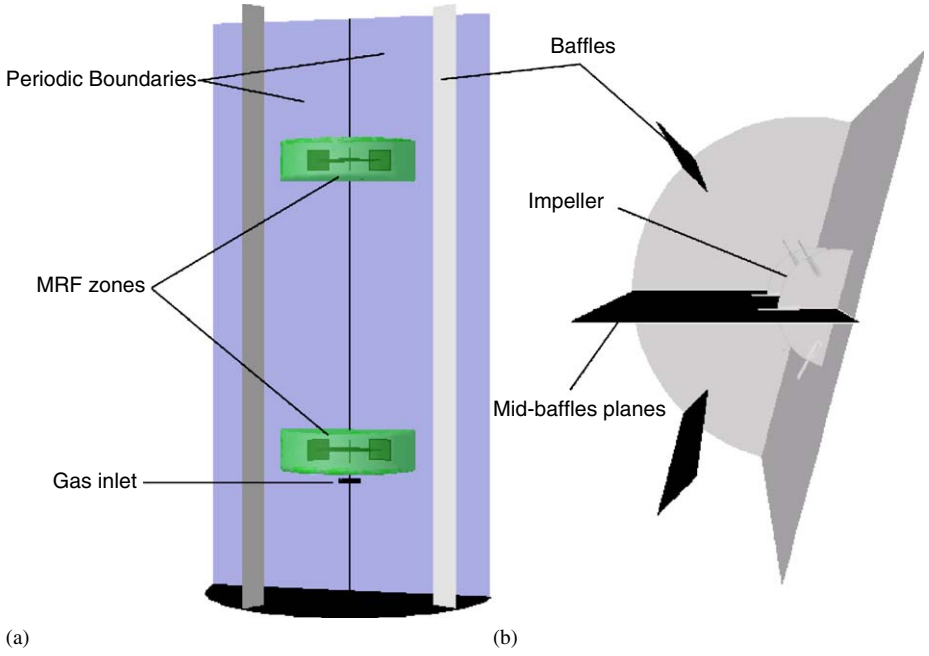

Fig. 1. (a) Solution domain (b) mid-baffles plane for numerical results and experimental sampling location.

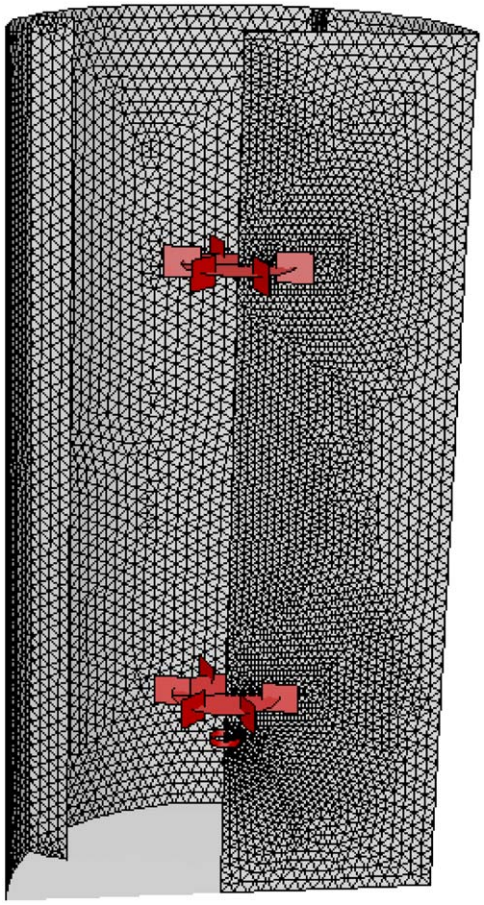

Fig. 2. Unstructured mesh used in the model.

acceptable (GAMBIT 2, 2004). The tank's domain is discretized by an unstructured finite volume method, obtained using the solver FLUENT 6.1. (2004) in order to convert the governing equations like continuity and momentum equations to algebraic equations that can be solved numerically. Periodic boundary condition is assumed in the left and right halves of the CFD model's symmetry plane to link the flow. The tank walls, the impeller surfaces and baffles are treated as nonslip boundaries with standard wall functions. The gas flow rate at the sparger is defined via inlet-velocity-type boundary condition with gas volume fraction equal to unity. The bubbles size at gas inlet depends on the sparger design, and the sparger design is beyond the scope of the present work. Nevertheless, the experimental data of Alves et al. (2002b) indicate that the bubble sizes vary between 0.5 and 4.0 mm. Considering these issues, the bubbles at the inlet are assumed to have a mean bubble size of 2.0 mm. At a liquid surface, a small gas zone is added at the free surface of water, a method that has been reported to diminish instabilities (FLUENT 6.1., 2004) and only gas is allowed to escape. The use of a MRF model enables a direct modeling of the impellers regions (Lane et al., 2002; Luo et al., 1994; Tabor et al., 1996) in a rotating frame of reference and the rest of tank in a stationary frame of reference. The MRF method represents a good compromise between physical accuracy and reasonable computational effort. The flow model is based on solving Navier–Stokes equations for the Eulerian–Eulerian multiphase model along with dispersed muliphase k–ε turbulent model. The governing differential equations are solved using iterative solution to the discrete form of the mathematical model using a PC-SIMPLE algorithm for pressure–velocity coupling with first order implicit formulation for unsteady integration and first-order upwind scheme discretization for spatial derivatives. Second order upwind failed to give a converged solution, maybe due to the complex flow physics and several coupling models. The gas and liquid are described as interpenetrating continua and equations for conservation of mass and momentum are solved for each phase. To avoid numerical difficulties, the transient calculations were made for two-phase flow starting with converged steady-state single primary phase flow field. The converged solution is assumed when the scaled residuals of all variables were smaller than 10^{-3}, the rate of gas entering and leaving must be equal and the pseudo-regime for holdup is reached.

2.2. Governing flow equations

FLUENT uses phase-weighted averaging for turbulent multiphase flow, and then no additional turbulent dispersion term is introduced into the continuity equation. Furthermore, there is no mass transfer between the air and water phases. The mass conservation equation for each phase is written as follows:

$$\frac{\partial}{\partial t}(\rho_i \alpha_i) + \nabla \cdot (\alpha_i \rho_i \vec{U}_i) = 0, \tag{1}$$

where ρ_i, α_i and $\vec{U}_i$ represent the density, volume fraction and mean velocity, respectively, of phase i (L or G). The liquid phase L and the gas phase G are assumed to share space in proportion to their volume such that their volume fractions sums to unity in the cells domain:

$$\alpha_L + \alpha_G = 1.0. \tag{2}$$

The momentum conservation equation for the phase i after averaging is written as follows:

$$\frac{\partial}{\partial t}(\rho_i \alpha_i \vec{U}_i) + \nabla \cdot (\alpha_i \rho_i \vec{U}_i \vec{U}_i) = -\alpha_i \nabla p + \nabla \cdot \bar{\bar{\tau}}_{\text{effi}} + \vec{R}_i + \vec{F}_i + \alpha_i \rho_i \vec{g}, \tag{3}$$

p is a pressure shared by the two phases and $\vec{R}_i$ represents the interphase momentum exchange terms. The term $\vec{F}_i$ represents the Coriolis and centrifugal forces applied in the rotating reference frame and is written as follows:

$$\vec{F}_i = -2\alpha_i \rho_i \vec{N} \times \vec{U}_i - \alpha_i \rho_i \vec{N} \times (\vec{N} \times \vec{r}). \tag{4}$$

The Reynolds stress tensor $\bar{\bar{\tau}}_{\text{effi}}$ is related to the mean velocity gradients using a Boussinesq hypothesis:

$$\bar{\bar{\tau}}_{\text{effi}} = \alpha_i(\mu_{\text{lam},i} + \mu_{t,i})(\nabla \vec{U}_i + \nabla \vec{U}_i^T) - \tfrac{2}{3}\alpha_i(\rho_i k_i + (\mu_{\text{lam},i} + \mu_{t,i})\nabla \cdot \vec{U}_i)\bar{\bar{I}}. \tag{5}$$

2.3. Interfacial momentum exchange

The most important interphase force is the turbulent drag force acting on the bubbles resulting from the mean relative velocity between the two phases and an additional contribution resulting from turbulent fluctuations in the volume fraction due to averaging of momentum equations (FLUENT 6.1., 2004). Other forces such as lift and added mass force may also be significant under the velocity gradient of the surrounding liquid and acceleration of bubbles, respectively. Both these forces and the turbulent part in the drag force have not been included in this paper. $\vec{R}_i$ is reduced only to the drag force proportional to the mean velocity difference, given by the following form:

$$\vec{R}_L = -\vec{R}_G = K(\vec{U}_G - \vec{U}_L) \tag{6}$$

K is the liquid–gas exchange coefficient written as follows:

$$K = \frac{3}{4}\rho_L \alpha_L \alpha_G \frac{C_D}{d}|\vec{U}_G - \vec{U}_L|, \tag{7}$$

d is the bubble diameter and C_D is the drag coefficient defined as function of the relative Reynolds number Re_p:

$$Re_p = \frac{\rho_L \mid \vec{U}_G - \vec{U}_L \mid d}{\mu_L}. \tag{8}$$

For calculation of the drag coefficient, the standard correlation of Schiller and Naumann is used (Ishii and Zuber, 1979):

$$C_D = \begin{cases} \dfrac{24(1 + 0.15Re_p^{0.687})}{Re_p} & Re_p \leqslant 1000.0, \\ 0.44 & Re_p > 1000.0. \end{cases} \tag{9}$$

However, this basic drag correlation applies to particles moving in a still liquid and do not necessarily apply to particles moving in turbulent liquid. In this work, a modified drag law that takes into account the effect of turbulence is used. It is based on a modified viscosity term in the relative *Reynolds number* (Bakker and Van Den Akker, 1994):

$$Re_p = \frac{\rho_L \mid \vec{U}_G - \vec{U}_L \mid d}{\mu_L + C\mu_{t,L}}. \tag{10}$$

C is the model parameter introduced to account for the effect of the turbulence in reducing slip velocity and is set to 0.3. A value that has been found in the present work to fit the experiment values of Alves et al. (2002a).

2.4. Turbulence model equations

As the secondary phase is dilute and the primary phase is clearly continuous, the dispersed k–ε turbulence model is used in this paper and solves the standard k–ε equations for the primary phase. The turbulent liquid viscosity $\mu_{t,L}$ in Eq. (5) is written as follows:

$$\mu_{t,L} = \rho_L C_\mu \frac{k_L^2}{\varepsilon_L}. \tag{11}$$

And is obtained from the prediction of the transport equations for the k_L and ε_L:

$$\frac{\partial}{\partial t}(\rho_L \alpha_L k_L) + \nabla \cdot \left(\alpha_L \rho_L \vec{U}_L k_L\right) = \nabla \cdot \left(\alpha_L \frac{\mu_{t,L}}{\sigma_k}\nabla k_L\right) + \alpha_L G_{k,L} - \alpha_L \rho_L \varepsilon_L \times + \alpha_L \rho_L \Pi_k L \tag{12}$$

$$\frac{\partial}{\partial t}(\rho_L \alpha_L \varepsilon_L) + \nabla \cdot \left(\alpha_L \rho_L \vec{U}_L \varepsilon_L\right) = \nabla \cdot \left(\alpha_L \frac{\mu_{t,L}}{\sigma_\varepsilon}\nabla \varepsilon_L\right) + \alpha_L \frac{\varepsilon_L}{k_L} \times (C_{1\varepsilon} G_{k,L} - C_{2\varepsilon}\rho_L \varepsilon_L) + \alpha_L \rho_L \Pi_{\varepsilon L} \tag{13}$$

G_{kL} is the rate of production of turbulent kinetic energy. Π_{kL} and $\Pi_{\varepsilon L}$ represent the influence of the dispersed phase on the continuous phase and are modeled following Elgobashi and Rizk (1989). C_μ, $C_{1\varepsilon}$, $C_{2\varepsilon}$, $C_{3\varepsilon}$, σ_k and σ_ε are parameters of the standard k–ε model. Their respective values are: 0.09, 1.44, 1.92, 1.2, 1.0 and 1.3. The turbulent quantities for the dispersed phase like turbulent kinetic energy and turbulent viscosity of the gas were modeled following Simonin and Viollet (1998), Mudde and Simonin (1999) using the primary phase turbulent quantities (FLUENT 6.1., 2004).

2.5. Bubble break-up and coalescence equation

The prediction of bubble size, formed in the stirred tank, is required for the calculation of interfacial area and interphase momentum exchange. To have a range of bubble sizes, the gas undergoes a complex phenomena that tend to break up and coalesce the gas bubbles as they move through the liquid. Break-up tends to occur when disruptive forces in the liquid are large enough to overcome the surface tension of the bubbles. Coalescence occurs when two or more bubbles collide and the film of liquid between them becomes thin and ruptures. The approach taken here is the change in bubble number density n due to breakage and coalescence mechanisms. The number density approach (Alves et al., 2002a; Bakker and Van Den Akker, 1994; Ishii et al., 2002; Lane et al., 2005, 2002; Millies and Dieter, 1999; Sun et al., 2004; Wu et al., 1998) is based on population balance theory (Prince and Blanch, 1990), but it requires less computational effort than the population balance classes. Rather than using several distribution functions for the size ranges, a single distribution function of particle sizes is assumed, thus only a single scalar transport equation is required for the overall number density distribution. This model, predicting a local volume equivalent mean bubble diameter, does not address the full complexity of such a complex process, where a local size distribution obviously exists. However, such an approach has been shown to represent satisfactorily the behavior of complex two-phase flows (Alves et al., 2002a; Lane et al. 2005, 2002; Ishii et al., 2002). Alves et al. (2002a) found, for small bubbles less than 5 mm, that the mean volume diameter is approximately equal to the mean sauter diameter ($d_{32} \backsimeq 0.8\, d_{43}$). As a surface mean diameter (sauter diameter) is the useful property

for interfacial area and mass transfer, predicting local interfacial area with present model is only limited to small bubbles. The bubble number density n is related to the gas holdup α_G and the average size d by

$$n = \frac{\alpha_G}{(\pi/6)d^3}. \tag{14}$$

From the values of n at each cell in the tank model, the local average bubble size d can be calculated and so is the drag. The conservation equation of bubble number density can be written as (Lane et al., 2002; Wu et al., 1998) follows:

$$\frac{\partial n}{\partial t} + \nabla \cdot \left(n\vec{U}_G\right) = S_{\text{br}} - S_{\text{co}}. \tag{15}$$

S_{br} and S_{co} are respectively the rates of bubble breakage and coalescence. Turbulence is the primary mechanism responsible for break-up and only the small eddies can break the bubbles, while the large ones transport the bubbles. The bubble break-up rate is considered to depend on the frequency of collisions between bubbles and eddies of a similar size (Wu et al., 1998) and can occur only when the *Weber number* exceeds a critical value. The reported value of We_{crit} of turbulent flows is 1.2 (Lane et al., 2002; Rigby et al., 1997). The Weber number is given by

$$We = \frac{\rho_L u_t^2 d}{\sigma}, \tag{16}$$

where u_t is the velocity of eddies in the inertial sub-range of turbulent eddy spectrum, and is given by

$$u_t = 1.4(\varepsilon d)^{1/3}. \tag{17}$$

Following Wu et al. (1998), an expression inspired from the gas kinetic theory can be written for bubble break-up rate when $We > We_{\text{crit}}$:

$$S_{\text{br}} = C_{\text{br}} n \frac{(\varepsilon d)^{1/3}}{d}\left(1 - \frac{We_{\text{crit}}}{We}\right)^{1/2} \exp\left(-\frac{We_{\text{crit}}}{We}\right). \tag{18}$$

Coalescence depends essentially on turbulent fluctuations and less on variation in rise velocity of different size bubbles and velocity gradients. These mechanisms force nearby bubbles to approach each other and lead to collision. In this paper, the coalescence is considered to occur in the case of binary collisions between bubbles and the expression of coalescence rate is given by Wu et al. (1998)

$$S_{\text{co}} = C_{\text{co}}\eta_{\text{co}} d^2 (\varepsilon d)^{1/3} n^2 \frac{1}{(1 - \alpha_G^{1/3})}, \tag{19}$$

where C_{br} and C_{co} are adjustable parameters. In order to fit experimental data of Alves et al. (2002a), these values are respectively set to 0.075 and 0.05. η_{co} is the coalescence efficiency, which is set to unity (Lane et al., 2002; Wu et al., 1998). The constant coalescence efficiency is only an approximation and the detailed expression for efficiency which takes into account the probability of coalescence is needed. The model parameters C_{br} and C_{co} are adjusted by comparing predicted local mean bubble size with data reported by Alves et al. (2002a). While

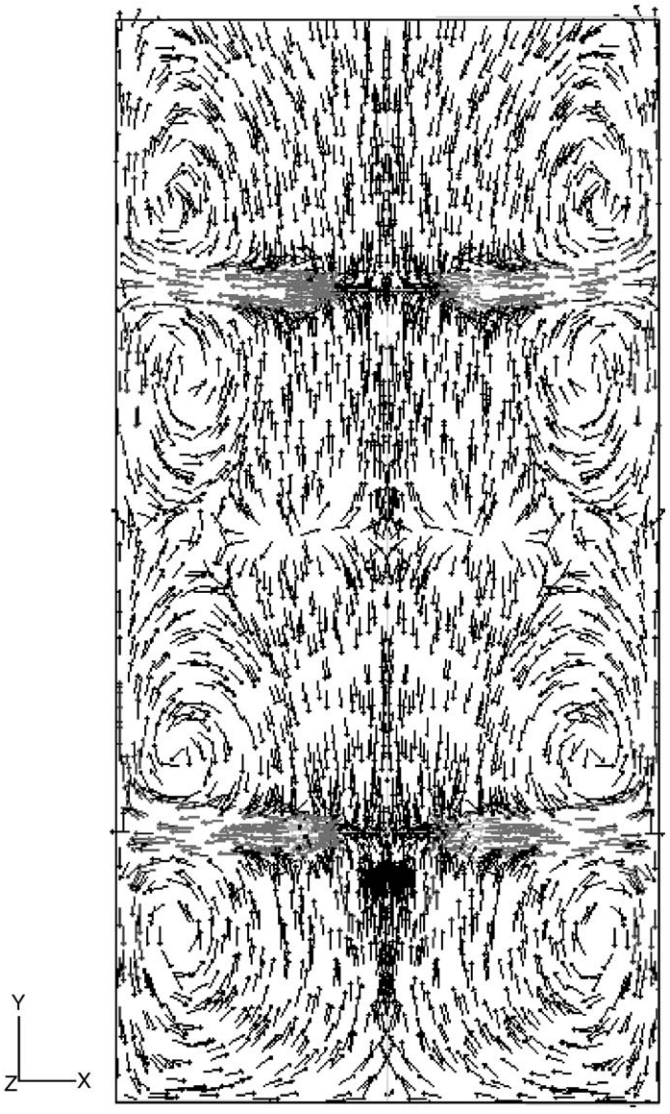

Fig. 3. Flow field for single liquid phase in the mid-plane between two baffles.

C is optimized by comparing predicted global gas holdup and local gas holdups with those from measurement of Alves et al. (2002a). Initially, C is guessed using the value of 0.22 from the work of Lane et al. (2002). Since gas holdup affects the bubble number density rates and inversely, the three parameters are dependent on each other and are readjusted successively in order to get the best numerical results for global gas holdup, local gas holdup and local mean bubble size.

3. Results and discussion

3.1. Flow pattern in gas–liquid flow

Fig. 3 illustrates the unaerated flow field, predicted by CFD in mid-plane between two baffles. The flow pattern is characterized by two independent induced circulation loops, above and below the discharge plane of the turbines (see Fig. 4). To provide a useful indication about the validity of simulation, the

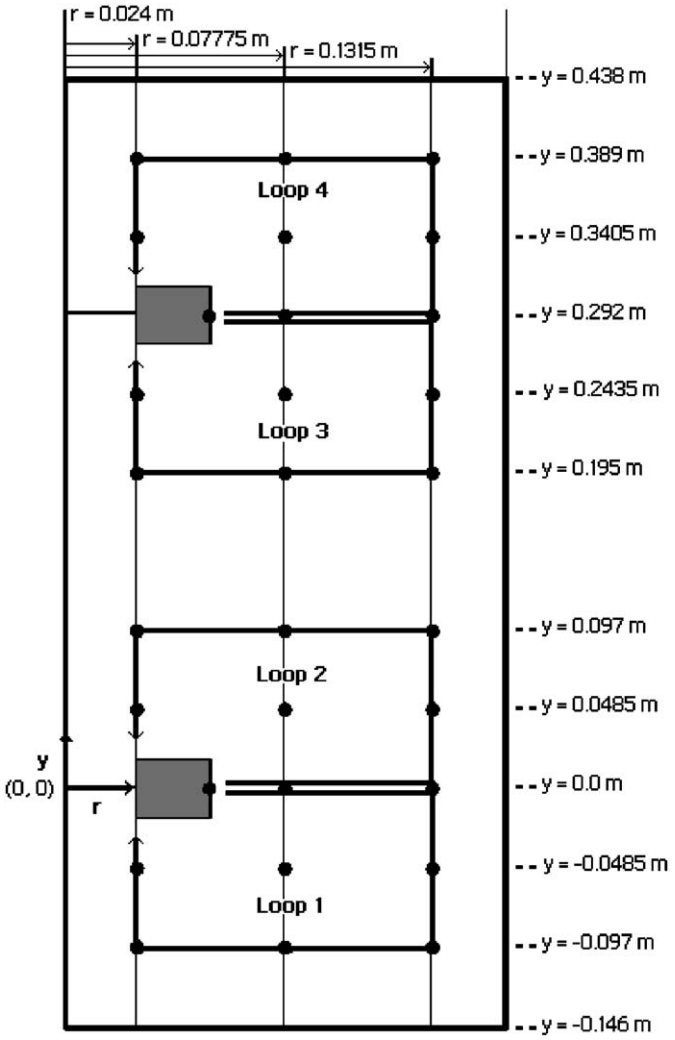

Fig. 4. Circulation loops in the mid-plane between two baffles with experimental points (•) from Alves et al. (2002a).

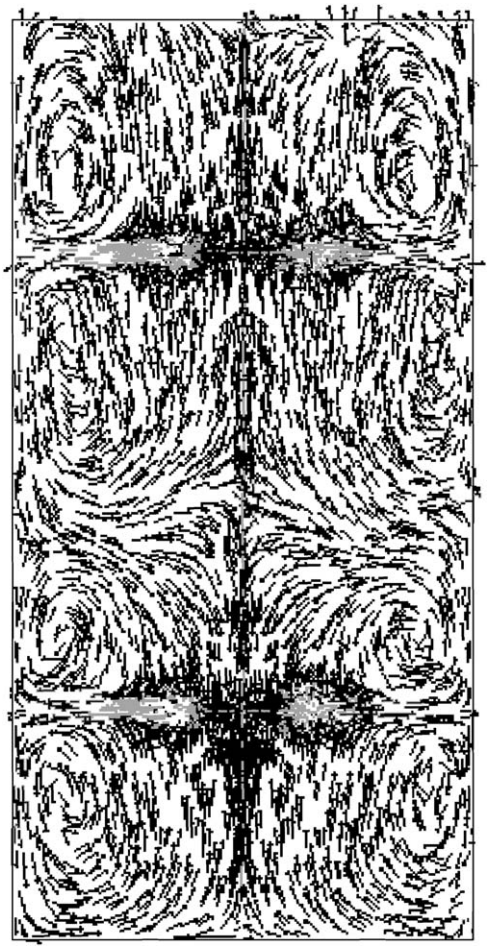

Fig. 5. Velocity vectors for two-phase flow in the mid-plane between two baffles. Left side: liquid phase; right side: gas phase.

predicted value of the pumping number N_Q and the circulation number N_C corresponding respectively to the turbine pumping flow rate Q_p and the circulation flow rate Q_C above and below the impeller are computed. The pumping number defined for each impeller is calculated by the integration of the flow rate discharged from the impeller between the lower and upper axial location of the blade:

$$N_Q = \frac{Q_p}{ND^3} = \frac{2\int_{-w/2}^{+w/2}\int_0^{\pi} \alpha_L R U_r \,\mathrm{d}\theta\,\mathrm{d}y}{ND^3}, \tag{20}$$

where U_r is the radial velocity, N is the impeller speed and D and R are respectively the impeller diameter and the impeller radius. For unareated conditions, N_Q is found to be 0.74 for the lower impeller and 0.75 for the upper one. These values are within the range of published data (0.75 ± 0.15 when $0.2 < D/T < 0.5$) (Micale et al., 1999; Rutherford et al., 1996). The circulation number is calculated from the integration carried out over the surface where the flow divides near the tank wall:

$$N_C = \frac{Q_C}{ND^3} = \frac{2\int_{R_i}^{T/2}\int_0^{\pi} \alpha_L r U_y \,\mathrm{d}\theta\,\mathrm{d}r}{ND^3}. \tag{21}$$

The lower integration limit R_i corresponds to the radial position where the flow begin to divide and U_y is the axial velocity. For unareated conditions the predicted value for the four loops is about 1.37 and the ratio N_C/N_Q is equal to 1.84 which is in agreement with the reported data (Vasconcelos et al., 1995). In the left side of Fig. 5, the liquid flow field in the case of aerated conditions is reported. The observed flow pattern corresponds very well with observations made by Alves et al. (2002a). The liquid flow circulation structure still follows the single-phase flow and the predicted ratio between aerated and unaerated pumping flow rates for both two impellers $(Q_p)_g/(Q_p)_u$ is found to be equal to the ratio predicted between gassed and ungassed power P_g/P. Their computed values are equal respectively to 0.76 an 0.75 which is in agreement with the assumption taken by Alves et al. (2002a) for the same setup. The power drawn by the two impellers is calculated as the product of the resistant torque (computed from the net moment on the two impellers) and angular velocity. The right side of

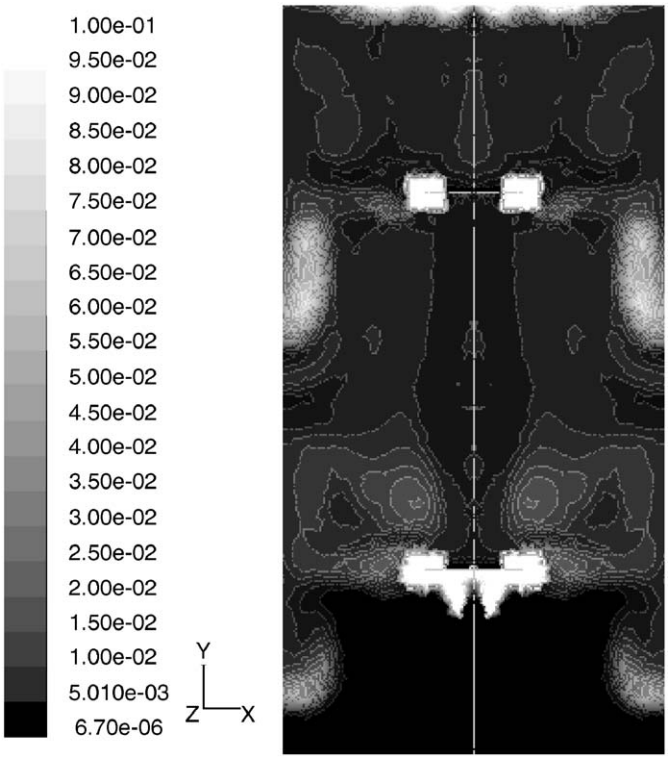

Fig. 6. Contours of gas volume fraction in the mid-plane between two baffles.

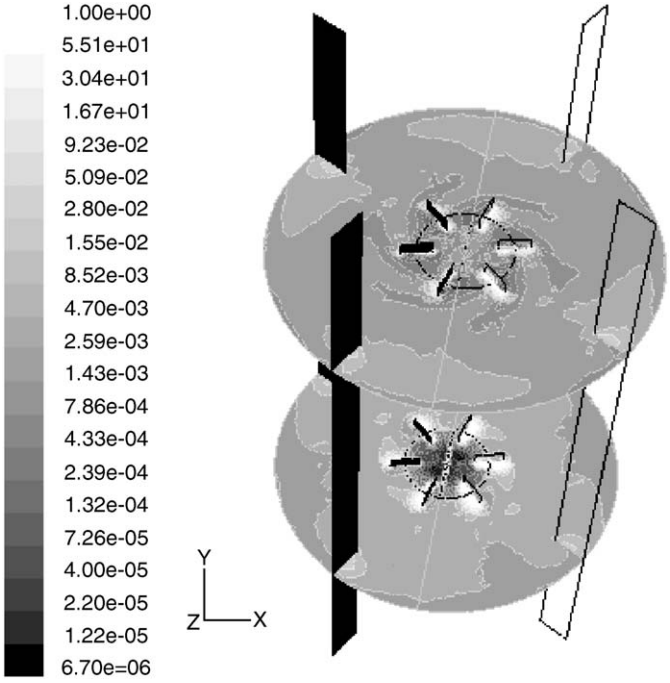

Fig. 7. Contours of gas volume fraction at the two impellers planes.

Fig. 5 shows the gas phase velocity field which follows the circulation of liquid flow field as the slip velocity is reduced by using modified drag correlation (Eqs. (9) and (10)). If only standard drag is used the pattern of gas flow field has been found to be very different from the measurements of Alves et al. (2002a) and the total gas holdup has been too low.

3.2. Gas holdup

Predicted gas volume fraction mid-plane between two baffles and in the plane of the impellers are given in Figs. 6 and 7. The pattern shows the gas accumulation in the recirculating flow regions and in the low-pressure region behind the impeller blades forming the so-called gas cavities. In the bottom of the tank under the lower impeller, the bubbles rise under the buoyancy forces which overcome the inertia effects and make the gas holdup much lower in this region. Figs. 8–10 show comparison between the present model's local gas holdup and the reported experimental and model data of Alves et al. (2002a) (see Fig. 4). Good agreement is found between the simulated results and experimental, except in the upper part of the vessel near the liquid-free surface where the local holdups predicted are lower than the measurements. This may be due to the choice of the drag correlation. The model of Alves et al. (2002a) seems to overpredict the local gas holdup essentially in the lower part of the vessel. The total gas holdup predicted by our CFD model is 2.3% compared to Alves's measurements of 2.5%, in contrast to its simpler model which gives 3.4%.

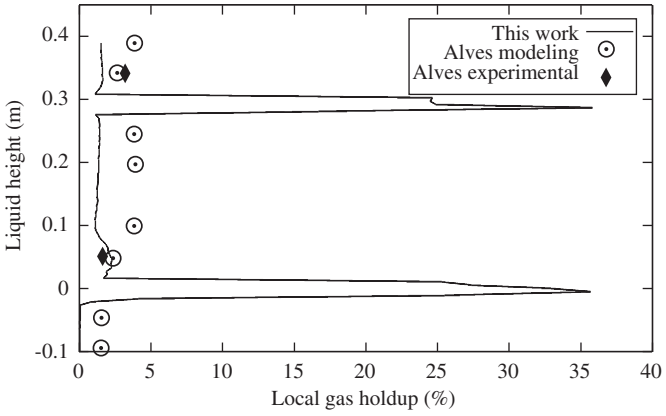

Fig. 8. Vertical profile of local gas holdup, in the mid-plane between two baffles, at radial position $r = 0.024$ m.

3.3. Bubble size distribution

The right side of Fig. 11 shows the predicted contours of local bubble size in a vertical mid-plane between two baffles. It can be seen that the smallest bubbles are found in the impeller discharge where the small eddies can break them (left side of Fig. 11). The eddies are represented by the integral length scale, which is a characteristic turbulence structure scale created by the impellers (Bakker and Van Den Akker, 1994; Jenne and Reuss, 1999). Above and below the impellers, the bubble size increases due to coalescence. Fig. 12 shows that bubbles are bigger behind the two impeller blades and baffles due to the high gas holdup there. At the blade edges, the drop in diameter indicated the break-up of the bubbles by intense turbulence. Figs. 13–16

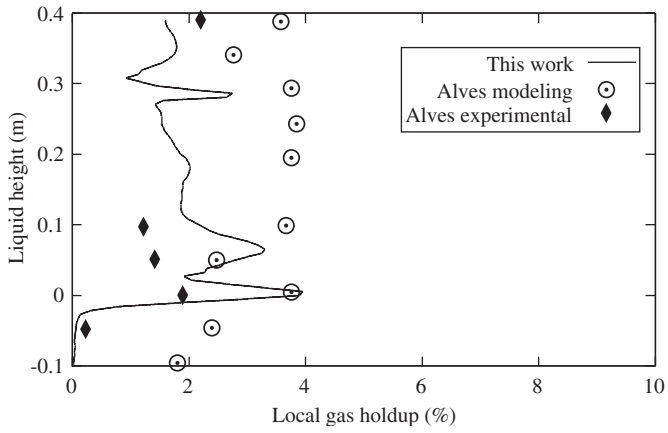

Fig. 9. Vertical profile of local gas holdup, in the mid-plane between two baffles, at radial position $r = 0.07775$ m.

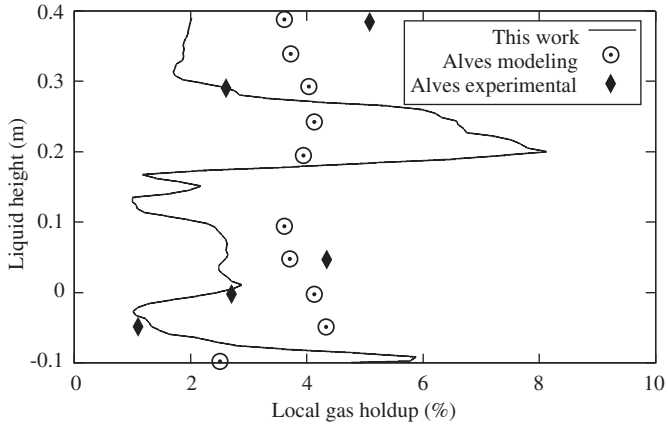

Fig. 10. Vertical profile of local gas holdup, in the mid-plane between two baffles, at radial position $r = 0.1315$ m.

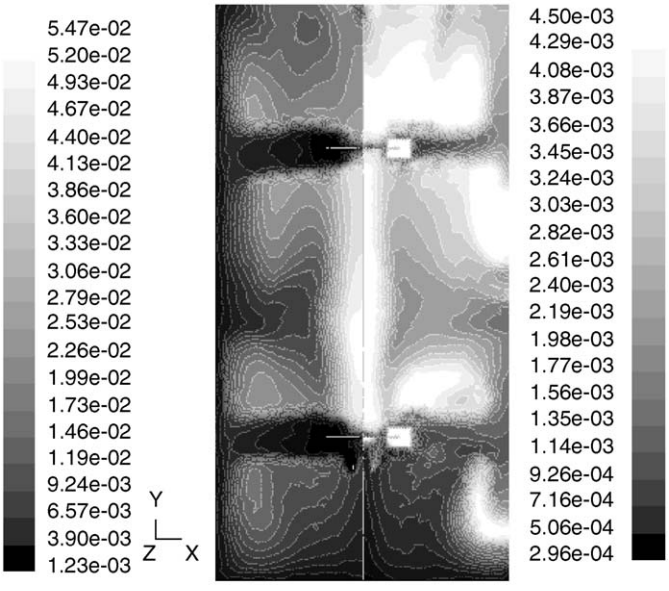

Fig. 11. Left: contours of turbulent length scale computed from $k^{3/2}/\varepsilon$ (m); right: contours of bubble diameter in the mid-plane between two baffles (m).

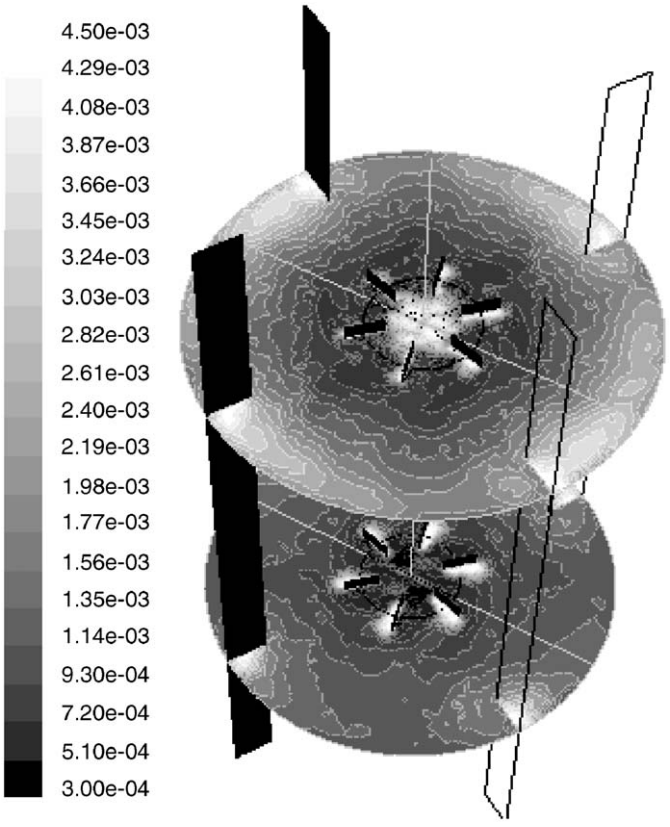

Fig. 12. Bubble diameter at the two impellers planes (m).

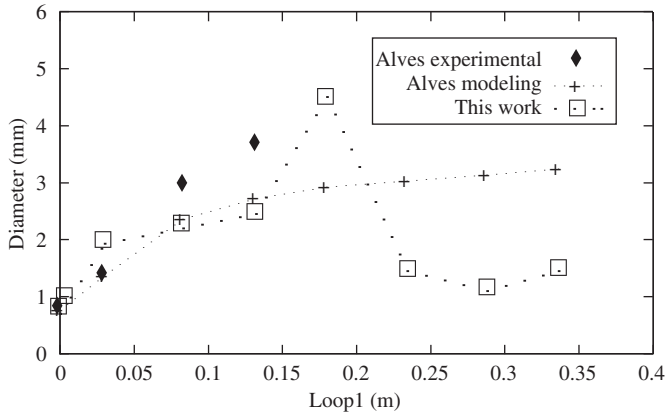

Fig. 13. Predicted bubble diameter along liquid circulation loop 1.

show quantitative agreements between predicted and experimental bubble size along the four circulation loops whose pathlines correspond to the work of Alves et al. (2002a,b) (see Fig. 4). In loop 2 and loop 4, the bubble size increases monotonically as the coalescence overcomes breakage in these circulations. In loop 3, large bubble size is located below the upper impeller consequence of bubble collisions caused by high accumulation of gas trapped inside the circulation near the wall. In circulation loop 1, it can be seen that bubble size increases from the impeller discharge until the wall where it become too large due to accumulation of gas in this region.

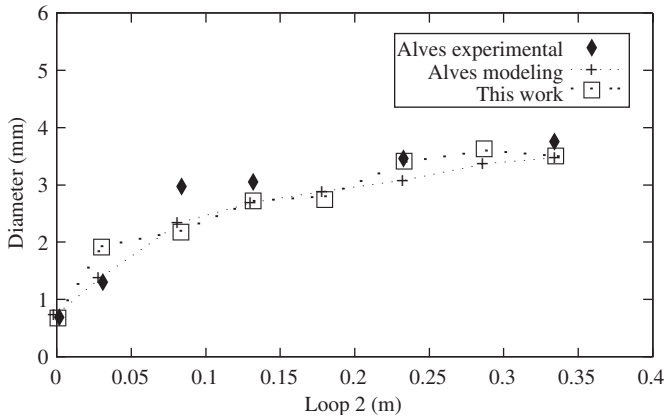

Fig. 14. Predicted bubble diameter along liquid circulation loop 2.

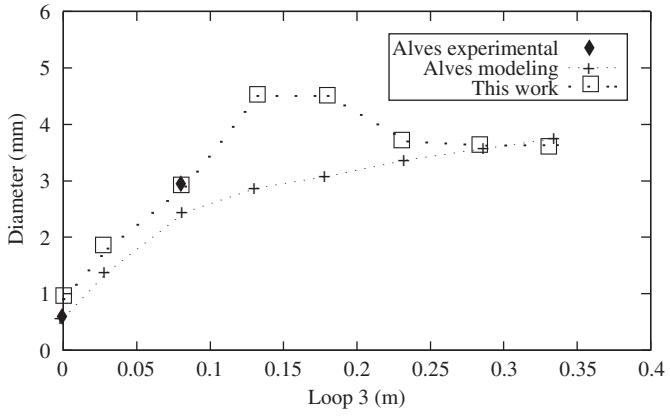

Fig. 15. Predicted bubble diameter along liquid circulation loop 3.

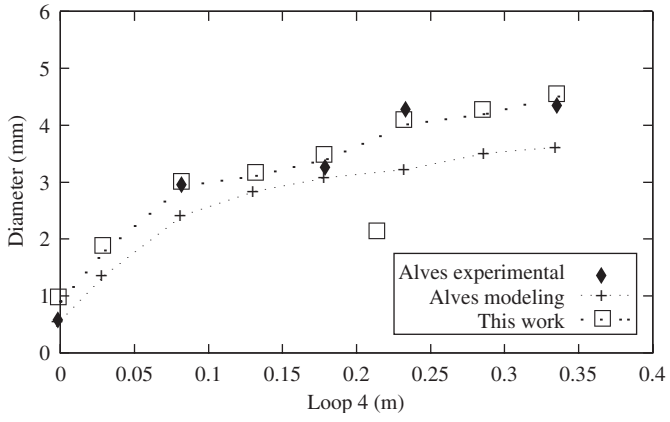

Fig. 16. Predicted bubble diameter along liquid circulation loop 4.

After that a decrease in bubble size is constated as the gas holdup decrease in the bottom of the tank. The model of Alves et al. (2002a) fails to predict bubble decrease at the end of loop 1 and 3 (see Alves et al., 2002a,b) this may be due to the high local gas holdups predicted with his coalescent model which leads to large bubbles. The disagreement may be caused by the very coarse grid used in the simple compartment model.

4. Conclusion

Turbulent two-phase flow with bubble break-up and coalescence are simulated in an aerated dual impeller stirred tank using a commercial CFD code. Three free parameters used in drag coefficient correlation and break-up and coalescence rates are adjusted to fit the detailed experimental data of Alves et al. (2002a). This set of data has been chosen because of its completeness and the quality of the measurements. We found this coefficients to be $C = 0.3$ for the modified drag correlation, $C_{\mathrm{br}} = 0.075$ for the break-up rate and $C_{\mathrm{co}} = 0.05$ for the coalescence rate. Predicted flow pattern, gas holdup and bubble size distributions are found to be in good quantitative agreement with the experimental findings. The mathematical model development is continuing by refining the interphase coupling and testing other turbulence models in order to provide a better agreement between predicted and experimental measurements.

Notation

C	model parameter
C_D	drag coefficient
d	bubble diameter, m
D	impeller diameter, m
$\vec{F}$	volumetric force, N m^{-3}
$\vec{g}$	acceleration due to gravity, m s^{-2}
H	liquid height, m
$\bar{\bar{I}}$	unit tensor
K	exchange coefficient, kg m^{-3} s^{-1}
l	width of the impeller blade, m
n	bubble number density, m^{-3}
$\vec{N}$	angular velocity, rad s^{-1}
p	pressure, N m^{-2}
P	power, W
$\vec{r}$	position vector, m
R	impeller radius, m
$\vec{R}$	interphase force, N m^{-3}
Re	Reynolds number
S	source sink, kg m^{-6} s^{-1}
t	time, s
T	tank diameter, m
u	root mean square turbulent velocity, m s^{-1}
$\vec{U}$	average velocity, m s^{-1}
w	impeller blade height, m
We	Weber number

Greek letters

α	volume fraction
ε	turbulent dissipation energy, m^2 s^{-3}
η_{co}	efficiency factor of coalescence, 1
μ	Viscosity, kg m^{-1} s^{-1}
ρ	density, kg m^{-3}
σ	surface tension, N m^{-1}
τ	characteristic time, s
$\bar{\bar{\tau}}$	stress tensor, kg m^{-1} s^{-2}

Subscripts

br	break-up
co	coalescence
crit	critical
eff	effective
G	gas phase
i	phase number; axis indexes of space coordinates
j	axis indexes of space coordinates
lam	laminar
L	liquid phase
t	turbulent

References

Alves, S.S., Maia, C.I., Vasconcelos, M.T., 2002a. Experimental and modelling study of gas dispersion in a double turbine stirred tank. Chemical Engineering Science 57, 487–496.

Alves, S.S., Maia, C.I., Vasconcelos, M.T., Serralheiro, A.J., 2002b. Bubble size in aerated stirred tank. Chemical Engineering Journal 89, 109–117.

Alves, S.S., Maia, C.I., Vasconcelos, M.T., 2004. Gas liquid mass transfer coefficient in stirred tanks interpreted through bubble contamination kinetics. Chemical Engineering and Processing 43, 823–830.

Bakker, A., Van Den Akker, H.E.A., 1994. A computational model for the gas–liquid flow in stirred reactors. Transactions of I.Chem.E. 72 (Part A), 594–606.

Deen, N.G., Solberg, T., Hjertager, B.H., 2002. Flow generated by an aerated Rushton impeller: two-phase PIV Experiments and numerical simulations. The Canadian Journal of Chemical Engineering 80, 1–15.

Elgobashi, S.E., Rizk, M.A., 1989. A two-equation turbulence model for dispersed dilute confined two-phase flows. International Journal of Multiphase Flow 15 (1), 119–133.

FLUENT 6.1., 2004. User's Manual to FLUENT 6.1. Fluent Inc. Centrera Resource Park, 10 Cavendish Court, Lebanon, USA.

Friberg, P.C., 1998. Three-dimensional modeling and simulations of gas–liquid flows processes in bioreactors. Ph.D. Thesis, Norwegian University of Science and Technology, Porsgrum, Norway.

GAMBIT 2, 2004. User's Manual to GAMBIT 2. Fluent Inc. Centrera Resource Park, 10 Cavendish Court, Lebanon, USA.

Hjertager, B.H., 1998. Computational fluid dynamics (CFD) analysis of multiphase chemical reactors. Trends in Chemical Engineering 4, 45–91.

Ishii, M., Zuber, N., 1979. Drag coefficient and relative velocity in bubbly, droplet or particulate flows. A.I.Ch.E. Journal 25 (5), 843–855.

Ishii, M., Kim, S., Uhle, J., 2002. Interfacial area transport equation: model development and benchmark experiments. International Journal of Heat Mass Transfer (45), 3111–3123.

Jenne, M., Reuss, M., 1999. A critical assessment on the use of *k–e* turbulence models for simulation of the turbulent liquid flow induced by Rushton-turbine in baffled stirred-tank reactors. Chemical Engineering Science 54, 3921–3941.

Khopkar, A.R., Rammohan, A.R., Ranade, V.V., Dudukovic, M.P., 2005. Gas–liquid flow generated by a Rushton turbine in stirred vessel: CARPT/CT measurements and CFD simulations. Chemical Engineering Science 60, 2215–2229.

Lane, G.L., Schwarz, M.P., Evans, G.M., 2002. Predicting gas–liquid flow in a mechanically stirred tank. Applied Mathematical Modeling 26, 223–235.

Lane, G.L., Schwarz, M.P., Evans, G.M., 2005. Numerical modelling of gas–liquid flow in stirred tank. Chemical Engineering Science 60, 2203–2214.

Luo, J.Y., Issa, R.I., Gosman, A.D., 1994. Prediction of impeller induced flows in mixing vessels using multiple frames of reference. IchemE Symposium Series, Institution of Chemical Engineers 136, 549–556.

Micale, G., Brucato, A., Grisafi, F., 1999. Prediction of flow fields in a dual-impeller stirred tank. A.I.Ch.E. Journal 45 (3), 445–464.

Millies, M., Dieter, M., 1999. Interfacial area density in bubbly flow. Chemical Engineering and Processing 38, 307–319.

Morud, K.E., Hjertager, B.H., 1996. LDA measurements and CFD modeling of gas–liquid flow in a stirred vessel. Chemical Engineering Science 51, 233–249.

Mudde, R., Simonin, O., 1999. Two- and three-dimensional simulations of a bubble plume using a two-fluid model. Chemical Engineering Science 54, 5061–5069.

Prince, M.J., Blanch, H.W., 1990. Bubble coalescence and break-up in air-sparged bubble columns. A.I.Ch.E. Journal 36 (10), 1485–1499.

Ranade, V.V., 1997. An efficient computational model for simulating flow in stirred vessels: a case of Rushton Turbine. Chemical Engineering Science 52, 4473–4484.

Ranade, V.V., Deshpande, V.R., 1999. Gas–liquid flow in stirred vessels: trailing vortices and gas accumulation behind impeller blades. Chemical Engineering Science 54, 2305–2315.

Rigby, G.D., Evans, G.M., Jameson, G.J., 1997. Bubble break-up from ventilated cavities in multiphase reactors. Chemical Engineering Science 52 (21/22), 2009–2025.

Rutherford, K., Lee, K.C., Mahmoudi, S.M.S., Yianneskis, M., 1996. Hydrodynamic characteristics of dual rushton impeller stirred vessels. A.I.Ch.E. Journal 42 (2), 332–346.

Simonin, C., Viollet, P.L., 1998. Predictions of an oxygen droplet pulverization in a compressible subsonic coflowing hydrogen flow. Numerical Methods for Multiphase Flows 1, 65–82.

Sun, X., Kim, S., Ishii, M., Beus, S., 2004. Modeling of bubble coalescence and disintegration in confined upward two-phase flow. Nuclear Engineering and Design (230), 3–26.

Tabor, G., Gosman, A.D., Issa, R.I., 1996. Numerical simulation of the flow in a mixing vessel stirred by a Rushton Turbine. IChemE Symposium Series 140, 25–34.

Vasconcelos, J.M.T., Alves, S.S., Barata, J.M., 1995. Mixing in gas–liquid contactors agitated by multiple turbines. Chemical Engineering Science 50 (14), 2343–2354.

Venneker, B.C.H., Derksen, J.J., Van Den Akker, H.E.A., 2002. Population balance modeling of aerated stirred vessels based on CFD. A.I.Ch.E. Journal 48 (4), 673–684.

Wu, Q., Kim, S., Ishii, M., Beus, S.G., 1998. One-group interfacial area transport in vertical bubbly flow. International Journal of Heat Mass Transfer 41 (8/9), 1103–1112.